Journal of Thermal Analysis and Calorimetry (2023) 148:14385–14403
https://doi.org/10.1007/s10973-023-12611-5

Thermal study of Darcy–Forchheimer hybrid nanofluid flow inside a permeable channel by VIM: features of heating source and magnetic field

Khaleeq ur Rahman[1] · Adnan[1] · Nidhish Kumar Mishra[2] · Mutasem Z. Bani-Fwaz[3]

Received: 27 July 2023 / Accepted: 19 September 2023 / Published online: 13 November 2023

Abstract

The nanofluids extensively contribute to cope the new heat transport challenges facing by the engineering systems and industries including paint, ceramics, chemical, aerodynamics, electronics, and medical sciences, etc. Thus, the innovations in new nanoliquid models can be disregarded in light of broad applications spectrum. Therefore, the current work concerns with the thermal process of hybrid nanoliquid by adding the important physical phenomenon. The flow of bionanofluid is taken inside a uniform expanding/contracting channel. To increase the model novelty, the significant influence of Lorentz forces, porous media, and heating source is added in the problem formulation. The resultant bionanofluid model is then analyzed via VIM (variational iteration method) and provided a deep discussion. It is inspected that unvarying expansion/contraction in the range of $\alpha = 1.0, 2.0, 3.0, 4.0$ and $\alpha = -1.0, -2.0, -3.0, -4.0$, the bionanofluid attained maximum velocity about the central portion and in rest of the part it declines. However, due to increased viscosity of hybrid nanofluid, it reduced rapidly than conventional nanofluid. By increasing the permeability from 0.1 to 0.4, a rapid decrease in the fluid movement is observed. Further, the heat transmission progress reduced against the porous medium and Lorentz forces. The heat generation effects boosted the heating performance of the hybrid nanofluid. Moreover, the skin friction and heat transport rate are also discussed.

Keywords Heat transfer · Porosity effects · Heat generation · Channel flow · Laminar flow

Abbreviations

$\widetilde{u}, \widetilde{v}$	Velocity components
$\widetilde{P}$	Pressure
ρ_b	Fluid density
ρ_{hbnf}	Density of hybrid nanofluid
k_b	Thermal conductivity of the basic fluid
k_{hbnf}	Thermal conductivity of hybrid nanofluid
μ_b	Dynamic of basic fluid
μ_{hbnf}	Dynamic viscosity of hybrid nanofluid
$\widetilde{T}$	Fluid temperature
σ_b	Electrical conductivity of basic fluid
σ_{hbnf}	Electrical conductivity of hybrid nanofluid
ϕ_1, ϕ_2	Nanoparticles mass concentration
M	Hartmann number
D_a	Darcy number
F_r	Forchheimer number
R_{e1}	Reynolds number
P_r	Prandtl number
Q	Heat generation number
C_{Fl}	Skin friction at the lower plate
C_{Fu}	Skin friction at the upper plate
N_{ul}	Nusselt number at the lower plate
N_{up}	Nusselt number at the upper plate

✉ Adnan
adnan_abbasi89@yahoo.com

[1] Department of Mathematics, Mohi-ud-Din Islamic University, Nerian Sharif 12080, AJ&K, Pakistan

[2] Basic Science Department, College of Science and Theoretical Studies, Saudi Electronic University, 11673 Riyadh, Saudi Arabia

[3] Department of Chemistry, College of Science, King Khalid University, P. O. Box 9004, 61413 Abha, Saudi Arabia

Introduction

Hybrid nanoliquid can be prepared from insertion of two sort of nanoparticles in the working host liquid. The thermal conductivity of resultant hybrid fluid ([1–3]) increased in the existence of cumulative nanoparticles effects. In 2014, Mustafa et al. [4] carried out a numerical study to examine the heat transport in convective nanofluid flow passing over a plate with existence of radiative heat flux. They applied Runge–Kutta fourth–fifth-order scheme for conversion of system equations using similarity transformation along with shooting technique. Role of various parameters has been discussed in the study. In 2017, Hosseinzadeh et al. [5] examined the effects of thermophoresis and Brownian phenomenon on magnetohydrodynamic nanofluid [6, 7] flow together with the heat transfer between two parallel plates. Homotopy perturbation method used to solve modeled system and results indicates that rise the Brownian motion parameter would source an increase in temperature field.

Recently, Rafique et al. [8] and Bilal et al. [9] made efforts toward the analysis of nanoliquid flows by put their focus on conventional nano and hybrid nanofluids types. They checked the nanoparticles structure and mutual aggregation of the metallic particles on the thermal transmission of the fluids. Further, the authors accommodated the influence of physical constraints and provided in-depth analysis on the momentum and thermal boundary layers. In 2023, Mishra et al. [10], Bhatti et al. [11], Zhang et al. [12], Kumar et al. [13], and Nidhish et al. [14] reported comprehensive investigations about the nanofluids behavior and their heating and coolant characteristics in various engineering domains and predicted suitable ranges of the physical constraints. Also, they addressed the geometries effects on the fluid behavior inside the thermal and momentum boundary layers regions. They concluded that nanofluids are comparatively better than common fluids, and rest of the generation such as hybrid and ternary nanofluids are more reliable than traditional nano and simple fluids. The most innovative analysis regarding the nanoliquids transport have been reported by potential researchers around the world. These discussed in Refs. [15–17], and the studies given therein. Some novel studies for unsteady squeezed hybrid nanoliquid model [18], fractional order simulation for the performance of Maxwell [19] and standard Couette flow [20] of nanoliquids, catalytic characteristics of gold nanoparticles [21], fractal fractional simulation [22] for couple stress liquids, and fractional ramped [23] investigation of nanoparticles have been reported.

In 2019, Sharma et al. [24] studied the MHD flow which is conducting electrically under magnetic field effects. Finite difference technique used to handle PDEs and concluded that rise in magnetic strength evidence to a reduction in the velocity profile. In 2020, Abbas et al. [25] studied about nanofluid flow (see Refs. [26, 27]) and to expand the thermophysical resources of heat transfer and convective flow for unsteady nanofluid under magnetic field properties. Homotopy analysis method technique is used as measured instrument and established admirable agreement for shape factors. In 2020, Zainal et al. [28] examined the magnetohydrodynamic hybrid nanoliquid in the presence of quadratic velocity flowing on stretching/shrinking sheet to study the change in convective heat transfer rate with stability analysis and also discovered the behavior of various influential parameters. In 2021, Akbar et al. [29] analyzed the temperature and velocity profile of inviscid flow by considering the effects of various variables parameters using continuity, energy, and momentum equations ([30–33]) model and displayed the findings in graphs and tables.

In 2021, Noor et al. [34] demonstrated the Buongiorno's nanofluid model to explore the Brownian motion and thermophoresis effects on Jeffery nanofluid flowing through a porous medium. Keller box method has been used to analyze the model. In 2021, Hussain et al. [35] conducted the study on hybrid nanofluid flow in the presence of convection condition over a rotating disk. The model has been designed to observe heat transfer behavior and thermophysical characteristics. This comparative study shows that hybrid nanofluid has been more effective. In 2021, Waqas et al. [36] presented the model to study the behavior of radiative hybrid nanofluid flow passing over a rotating disk by considering various parameters impact. The outcomes of the study have been shown through graphs. In 2021, Ahammad et al. [37] reconnoitered the phenomenon of entropy in a spongy plate placed vertically and considering the suction velocity and magnetohydrodynamic effect [38]. The analysis of entropy generation and the influential effect of various parameters have been discussed in detail. They found the results using finite difference method.

In 2021, Abdullah et al. [39] analyzed the fluid flow behavior with electrical conduction by formulating the desired model for investigation. The fluid flow was observed in porous medium between parallel plates under normal Lorentz forces influence. The fixed pressure gradient and thermal flux have been applied. The finite difference method and eigen function expansion method have been used to find the solutions of the equations. In 2022, Rashad et al. [40] reconnoitered thermal transmission for EPF (Eyring–Powel fluid) hybrid nanofluid [41] under the effect of variable temperature and velocity. The transformation of governing equations has been done through RKF45 with shooting technique. The study has been found useful in various industrial processes. In 2022, Yaseen et al. [42] deliberated the study between symmetrical squeezing mono nanofluid and hybrid nanofluid (see Refs. [43–46]) in permeable medium under the effect of heat transportation. The outcomes of this study have been used in many industrial areas for cooling and heating process.

In 2023, Abbas et al. [47] observed the Dufour and Soret impact in addition with the effects of second-order slip and thermal slip for Maxwell fluid flow. They illustrated the results for various parameters through graphs and tables after transforming the equations through numerical method. In 2022, Lenci et al. [48] examined the inertial flow in porous surface which is governed by the Forchheimer equation. The association was realistic to the mean permeability which shows that it rises (declines) with increasing (decreasing) exponent for flow vertical (horizontal) to layers. In 2022, Elbashbeshy et al. [49] studied about the gyrotactic movement. The model treated numerically and concluded that permeability parameter repels the thickness of thermal boundary layer. Some latest studies for nanofluid have been reported in Refs. [50, 51].

The keen observations from the above listed literature, it is pointed that the innovative study of hybrid nanoliquids (see Refs. [52–54]) flowing inside a channel formed by two porous plates under the potential influence of Lorentz forces, porosity, and internal heating source is presented so far. Therefore, this attempt is made to investigate the behavior and transport of heat in hybrid nanoliquids due to the bunch of physical parametric effects. The acquired model will be analyzed via VIM and then organized the physical results according to the model domain. The study will helpful to adjust the strength of physical parameters for the estimation of better model results. In the first step, development of the model will be done via supportive nanofluids correlations and transformative rules. After that the achievement of the model, the variational iteration method will be exercised for the mathematical analysis and simulation of the physical results. After successfully implementation of the method, the results under increasing values of the included parameters will be demonstrated and then discussed comprehensively in the view of physical facts behind them.

Model development

Working domain

Let us considered the two parallel permeable plates in which hybrid nanofluid is flowing. Both the surfaces are located at $a(t)$ and $-a(t)$ along y-direction, respectively. It is assumed that the x, y directions have the velocity constituents as u and v. Further, the model is associated to the features of source of heating, spongy media, and Lorentz forces. The heat absorption/generation term considered in the temperature equation. Using similarity transforms, the consequential hybrid nanofluid model will be attained. Physical formation for hybrid nanoliquid model is shown in Fig. 1.

The major assumptions which are essential in the problem formulation are that the functional fluid possesses the characteristics of incompressibility, viscous, and laminar flow. The walls are subject to the uniform expansion/contraction and constant fluid injected from each wall. Moreover, the working suspension is homogeneous, and the hybrid nanoparticles added up to 0.6% in the base

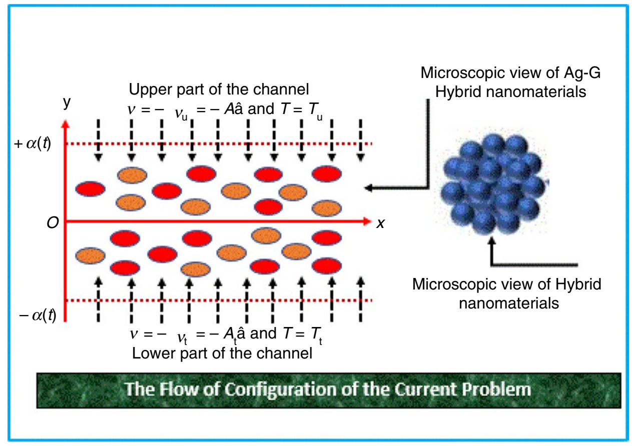

Fig. 1 The flow of (Ag-G)/blood hybrid nanoliquid along increasing direction of x

solvent. Further, the influence of porosity, Lorentz forces, and heating source in the energy equation is the significant insights in the problem development.

The flow sequence comprising the Darcy–Forchheimer impacts [55], magnetic field, and heating source is depicted in Fig. 1 which can be represented by the following physical laws in the form of following constitutive model:

$$\frac{\partial \widetilde{u}}{\partial x}+\frac{\partial \widetilde{v}}{\partial y}=0, \tag{1}$$

$$\rho_{\mathrm{hbnf}}\left(\frac{\partial \widetilde{u}}{\partial t}+\widetilde{u}\frac{\partial \widetilde{u}}{\partial \widetilde{x}}+\widetilde{v}\frac{\partial \widetilde{u}}{\partial \widetilde{y}}\right) = -\frac{\partial \widetilde{P}}{\partial \widetilde{x}}+\mu_{\mathrm{hbnf}}\left[\frac{\partial^2 \widetilde{u}}{\partial \widetilde{x}^2}+\frac{\partial^2 \widetilde{u}}{\partial \widetilde{y}^2}\right] - \sigma_{\mathrm{hbnf}}{B_0}^2\widetilde{u}-\frac{\nu_{\mathrm{hbnf}}}{K^*}\widetilde{u}-\frac{C_{\mathrm{b}}\widetilde{u}^2}{\sqrt{K^*}}, \tag{2}$$

$$\rho_{\mathrm{hbnf}}\left(\frac{\partial \widetilde{v}}{\partial t}+\widetilde{u}\frac{\partial \widetilde{v}}{\partial \widetilde{x}}+\widetilde{v}\frac{\partial \widetilde{v}}{\partial \widetilde{y}}\right) = -\frac{\partial \widetilde{P}}{\partial \widetilde{y}}+\mu_{\mathrm{hbnf}}\left[\frac{\partial^2 \widetilde{v}}{\partial \widetilde{x}^2}+\frac{\partial^2 \widetilde{v}}{\partial \widetilde{y}^2}\right] - \sigma_{\mathrm{hbnf}}{B_0}^2\widetilde{v}-\frac{\nu_{\mathrm{hbnf}}}{K^*}\widetilde{v}-\frac{C_{\mathrm{b}}\widetilde{v}^2}{\sqrt{K^*}}, \tag{3}$$

$$\left(\rho C_{\mathrm{p}}\right)_{\mathrm{hbnf}}\left(\frac{\partial \widetilde{T}}{\partial t}+\widetilde{u}\frac{\partial \widetilde{T}}{\partial \widetilde{x}}+\widetilde{v}\frac{\partial \widetilde{T}}{\partial \widetilde{y}}\right) = k_{\mathrm{hbnf}}\left[\frac{\partial^2 \widetilde{T}}{\partial \widetilde{x}^2}+\frac{\partial^2 \widetilde{T}}{\partial \widetilde{y}^2}\right]+Q_0\left(\widetilde{T}-\widetilde{T}_0\right), \tag{4}$$

The associated model conditions are as follows:

$$\begin{cases} \widetilde{u} = 0, T = T_l, \widetilde{v} = -v_l = -hA_l & \text{at} \quad \widetilde{y} = -h(t), \\ \widetilde{u} = 0, T = T_u, \widetilde{v} = -v_u = -hA_u & \text{at} \quad \widetilde{y} = h(t), \end{cases} \tag{5}$$

Now, we suggest;

$$\chi = \frac{\partial \widetilde{v}}{\partial \widetilde{x}} - \frac{\partial \widetilde{u}}{\partial \widetilde{y}}, \tag{6}$$

To remove the pressure influence and essential derivatives yield the following form:

$$\rho_{\text{hbnf}}\left(\frac{\partial \widetilde{\chi}}{\partial t} + \widetilde{u}\frac{\partial \widetilde{\chi}}{\partial \widetilde{x}} + \widetilde{v}\frac{\partial \widetilde{\chi}}{\partial \widetilde{y}}\right) = \mu_{\text{hbnf}}\left[\frac{\partial^2 \widetilde{\chi}}{\partial \widetilde{x}^2} + \frac{\partial^2 \widetilde{\chi}}{\partial \widetilde{y}^2}\right], \tag{7}$$

In the result of Eq. (7), we arrived with Eq. (8).

$$\rho_{\text{hbnf}}\left(\widetilde{u}_{\text{yt}} + \widetilde{u}\widetilde{u}_{\text{yx}} + \widetilde{v}\widetilde{u}_{\text{yy}}\right) = \mu_{\text{hbnf}}\widetilde{u}_{\text{yyy}}, \tag{8}$$

Now, we introducing the consequent transform variables for further simplification of our model:

$$y = \eta h, \tag{9}$$

$$\tilde{u} = \frac{\upsilon f\, \tilde{x}\tilde{f}_\eta}{h},\ \tilde{v} = -\frac{\upsilon f\, \tilde{f}(\eta,t)}{h^2},\ \tilde{\psi} = -\frac{\upsilon f\, \tilde{x}\tilde{f}(\eta,t)}{h}, \beta(\eta) = \frac{\tilde{T} - \tilde{T}_u}{\tilde{T}_i - \tilde{T}_u}, \tag{10}$$

Now, the further assumptions on the previous BCs income the following version:

$$\begin{cases} \widetilde{f}_\eta = 0, \widetilde{f} = R_{e}, Re1 = \frac{hh \cdot A_u}{\upsilon_f} \text{ at } \eta = -1, \\ \widetilde{f}_\eta = 0, \widetilde{f} = R_{e}, Re1 = \frac{hh \cdot A_u}{\upsilon_f} \text{ at } \eta = 1, \end{cases} \tag{11}$$

Here, R_{e1} is associated to the permeation effects which is corresponds to positive and negative values. Further, the second set of transformations is enlisted in Eq. (12).

$$x = \frac{\widetilde{x}}{h}, u = \frac{\widetilde{u}}{h}, v = \frac{\widetilde{v}}{h}, f = \frac{\widetilde{f}}{Re_1}, \tag{12}$$

Nanofluid characteristics

The following hybrid thermophysical properties are utilized in the formation of nanofluid and for the computation against increasing mass concentration.

$$\hat{\rho}_{\text{hbnf}} = (1 - \mho_2)\left[(1 - \mho_1) + \mho_1\left(\frac{\rho_{s_1}}{\rho_b}\right)\right] + \mho_2\left(\frac{\rho_{s_2}}{\rho_b}\right),$$

$$(\hat{\rho}C_p)_{\text{hbnf}} = (1 - {}_2)\left[(1 - {}_1) + {}_1\frac{(\hat{\rho}C_p)s_1}{(\hat{\rho}C_p)_b}\right] + {}_2\frac{(\hat{\rho}C_p)s_2}{(\hat{\rho}C_p)_b},$$

$$\mu_{\text{hbnf}} = \frac{1}{(1 - \mho_1)^{2.5}(1 - \mho_2)^{2.5}},$$

$$\left.\begin{aligned} \frac{\hat{k}_{\text{hbnf}}}{\hat{k}_{\text{bnf}}} &= \frac{\hat{k}_{s_2} + 2\hat{k}_{\text{bnf}} - 2_2(\hat{k}_{\text{bnf}} - \hat{k}_{s_2})}{\hat{k}_{s_2} + 2\hat{k}_{\text{bnf}} + _2(\hat{k}_{\text{bnf}} - \hat{k}_{s_2})} \\ \frac{\hat{k}_{\text{bnf}}}{\hat{k}_b} &= \frac{\hat{k}s_1 + 2\hat{k}_b - 2_1(\hat{k}_b - \hat{k}s_1)}{\hat{k}s_1 + 2\hat{k}_b + _1(\hat{k}_b - \hat{k}s_1)} \end{aligned}\right\},$$

$$\left.\begin{aligned} \frac{\hat{\sigma}_{\text{hbnf}}}{\hat{\sigma}_{\text{bnf}}} &= \left(\frac{\hat{\sigma}s_2 + 2*\hat{\sigma}_{\text{bnf}} - 2_2(\hat{\sigma}_{\text{bnf}} - \hat{\sigma}s_2)}{(\hat{\sigma}s_2 + 2\hat{\sigma}_{\text{bnf}} + _2(\hat{\sigma}_{\text{bnf}} - \hat{\sigma}s_2)}\right. \\ \frac{\hat{\sigma}_{\text{bnf}}}{\hat{\sigma}_b} &= \left(\frac{\hat{\sigma}s_1 + 2*\hat{\sigma}_b - 2_1(\hat{\sigma}_b - \hat{\sigma}s_1)}{(\hat{\sigma}s_1 + 2\hat{\sigma}_b + _1(\hat{\sigma}_b - \hat{\sigma}s_1)}\right. \end{aligned}\right\},$$

Here, $\mho_1, \mho_2$ designate the particles mass ϕ_1 and ϕ_2, respectively. The values of the characteristics used are portrayed in Fig. 2a–c, respectively. Graphically, it is revealed that the nanoparticle GO (graphene oxide) has utmost thermal conductivity and heat capacity correlate to nanoparticle Ag, while the nanoparticle Ag has high density as compared to nanoparticle GO (graphene oxide). Figure 3a–d depicts the significant changes in the characteristics of bionanofluid when the mass concentration rises from 0.01% to 0.06%. Further, the specific value for the working components is given in Table 1.

Finally, the following model acquired:

$$F'''' + \frac{\frac{\hat{\rho}_{\text{hbnf}}}{\hat{\rho}_b}}{\frac{\hat{\mu}_{\text{hbnf}}}{\hat{\mu}_b}}\left(\alpha\left(\eta F''' + F''\right) + R_{e1}\left(FF''' - F'F''\right)\right) - M\frac{\frac{\hat{\sigma}_{\text{hbnf}}}{\hat{\sigma}_b}}{\frac{\hat{\mu}_{\text{hbnf}}}{\hat{\mu}_b}}F'' - F''D_a - \frac{\frac{\hat{\rho}_{\text{hbnf}}}{\hat{\rho}_b}}{\frac{\hat{\mu}_{\text{hbnf}}}{\hat{\mu}_b}}F_r R_{e1}F''F' = 0, \tag{13}$$

$$F(-1) - s = 0, F'(-1) = 0, F(1) = 0, \tag{14}$$

The refined energy model is as follows:

$$\frac{\widehat{k}_{\text{hbnf}}}{\widehat{k}_b}\beta'' + \frac{\text{P}_r(\widehat{\rho}C_p)_{\text{hbnf}}}{(\widehat{\rho}C_p)_b}\left(\alpha\eta\beta' + R_{e1}F\right) + Q\text{P}_r\beta = 0, \tag{15}$$

$$\beta(-1) = 1, \beta(1) = 0, \tag{16}$$

Shear drag and Nusselt number

For the current model, the local thermal gradient and drag force are expressed in the following equations:

$$C_F = \frac{\tau a(t)}{\widehat{\rho}_{\text{hbnf}}v_1^2}, \tau_w = \mu_{\text{hbnf}}\left[\frac{\partial \widetilde{u}}{\partial y}\right] \quad \text{when } y = \mp a, \tag{17}$$

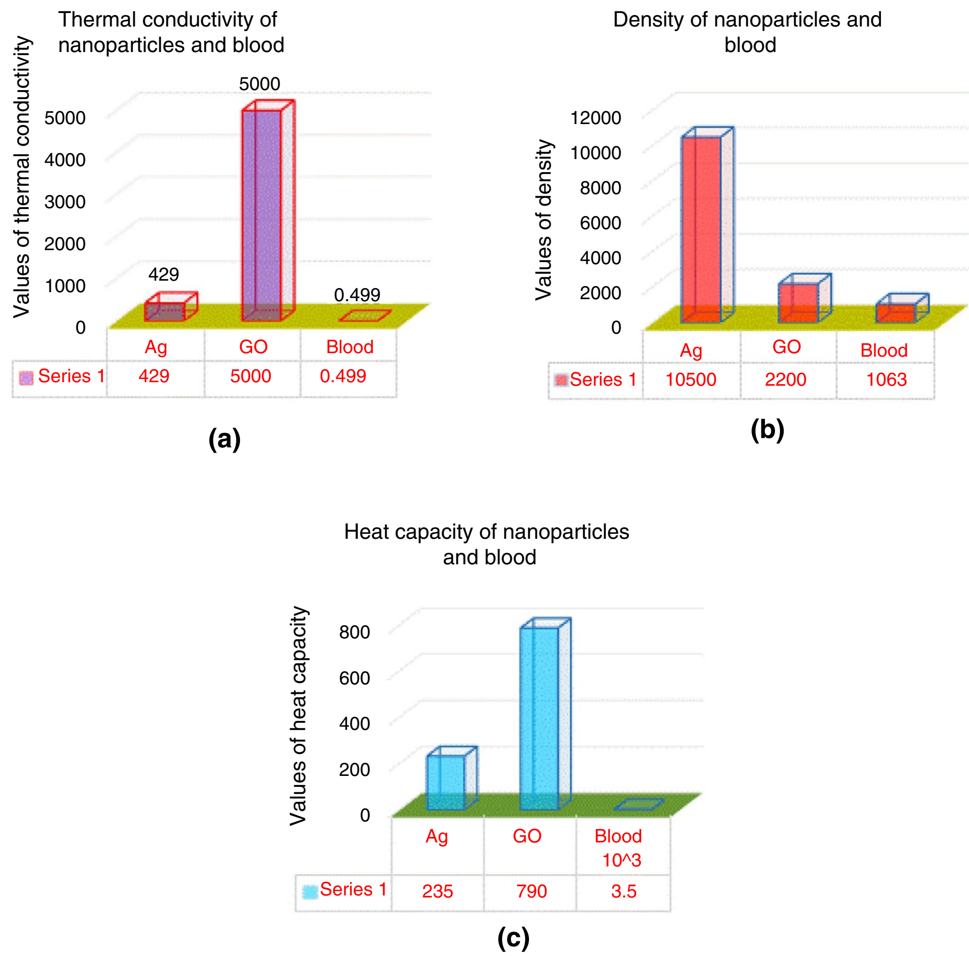

Fig. 2 Properties of Ag, Go, and blood used in this study

$$N_{\rm u} = \frac{a}{k_{\rm f}(T_{\rm l} - T_{\rm u})}\left[k_{\rm hbnf}\frac{\partial T}{\partial y} + q_{\rm rd}\right], \tag{18}$$

These yield the formulas:

$$R_{\rm l}^2 C_{\rm Fl} = \frac{\left[(1 - {}_1)^{2.5}(1 - {}_2)^{2.5}\right]^{-1}}{\left[(1 - {}_2)\left[(1 - {}_1) + {}_1\left(\frac{\rho_{S_1}}{\rho_{\rm b}}\right)\right] + {}_2\left(\frac{\rho_{S_2}}{\rho_{\rm b}}\right)\right]}F''(-1), \tag{19}$$

$$R_{\rm u}^2 C_{\rm Fu} = \frac{\left[(1 - \phi_1)^{2.5}(1 - \phi_2)^{2.5}\right]^{-1}}{\left[(1 - \phi_2)\left[(1 - \phi_1) + \phi_1\left(\frac{\rho_{S_1}}{\rho_{\rm b}}\right)\right] + \phi_2\left(\frac{\rho_{S_2}}{\rho_{\rm b}}\right)\right]}F''(1), \tag{20}$$

$$\widetilde{N}_{\rm ul} = |\beta'(-1)|\frac{\widehat{k}_{\rm hbnf}}{\widehat{k}_{\rm b}}, \tag{21}$$

$$\widetilde{N}_{\rm up} = |\beta'(1)|\frac{\widehat{k}_{\rm hbnf}}{\widehat{k}_{\rm b}}, \tag{22}$$

Mathematical analysis

The VIM, often known as variational iteration method, is an illustrious semi-analytical scheme which is useful for the solution of classical as well as modern heat transfer problems. This scheme can be allowed for the tackling of both ordinary and partial differential equation models equally. The key advantage of the technique falls in its flexibility and its applicability in solving nonlinear nanofluid models. Primarily, the selection of initial guesses and Lagrange multiplier is the key to initiate the scheme. These two factors depend on the order and boundary conditions of the concerned model. Further, the scheme works by depending on the recursive relation, and high accuracy is corresponds to the maximum number of iterations.

Thus, the variational iteration method is selected to investigate the physical results based on their less computational cost and remarkable accuracy. This method is very useful to tackle such type of bionanofluid models. The desired solutions can be achieved up to higher order accuracy by increasing the number of iterations. The complete working procedure of this technique is elaborated below, and the model is coded according to the following steps.

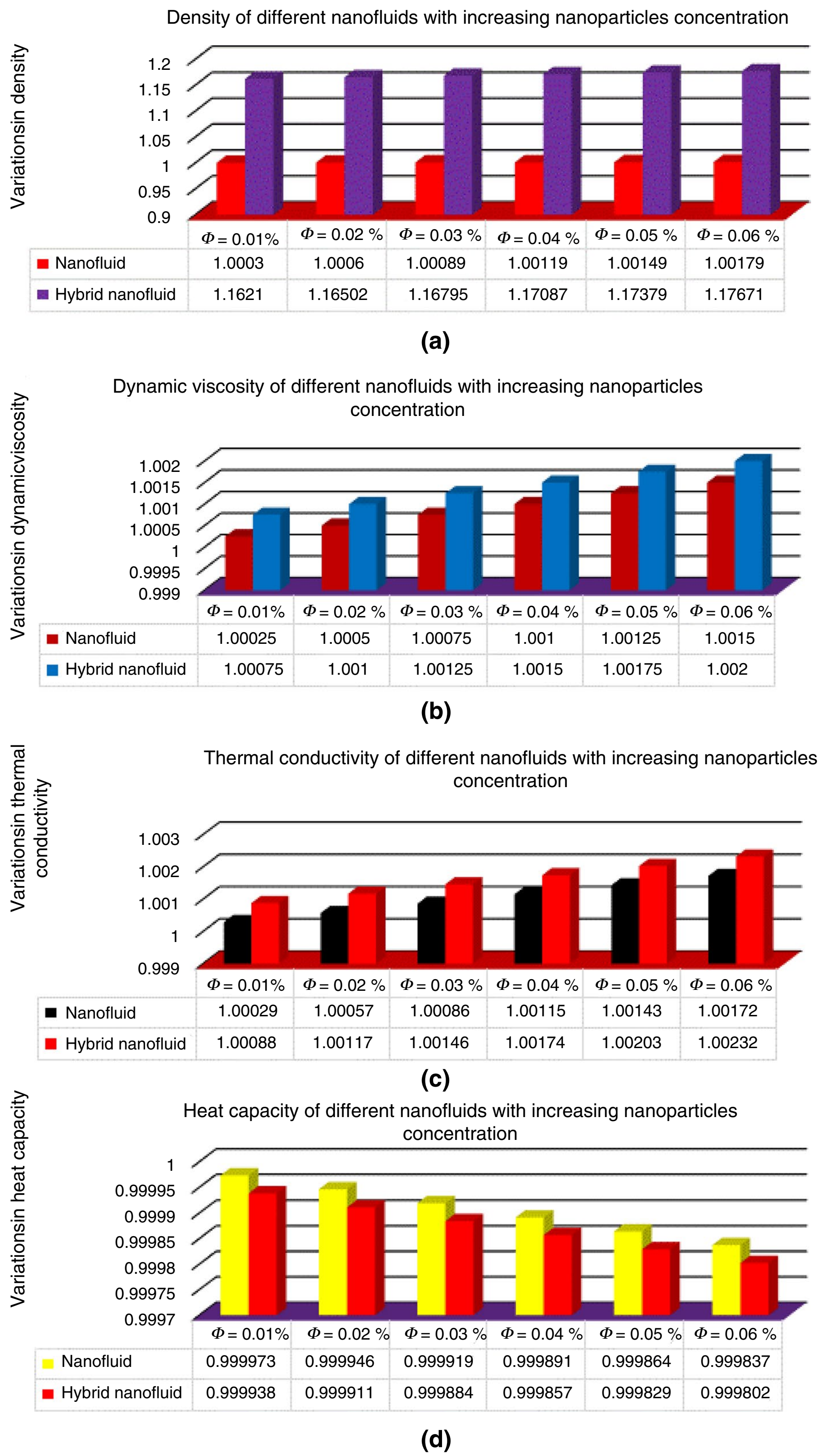

Fig. 3 Comparison of nanofluid and hybrid nanofluid properties against increasing mass concentration

Table 1 The characteristics values of the basic solvent and nanoparticles

Basic fluid/nano-sized particles	Characteristic values			
	ρ	C_p	k	σ
Blood	1063	3594	0.499	5.5×10^{-6}
Graphene	2200	790	5000	35×10^{-6}
Ag (spherical)	10500	235	429	59.6×10^{-6}

The model is arranged in the subsequent pattern which indicates the linear operators ($\overbrace{\mathcal{L}_{01}}$, $\overbrace{\mathcal{L}_{02}}$), nonlinearities ($\overbrace{\mathcal{R}_{01}}$, $\overbrace{\mathcal{R}_{02}}$), linear factors ($\overbrace{\mathcal{N}_{01}}$, $\overbrace{\mathcal{N}_{02}}$), and nonhomogeneous factors ($\overbrace{q^*_{01}}$, $\overbrace{q^*_{02}}$).

$$\widehat{\mathcal{L}}_{01}F+\widehat{\mathfrak{R}}_{01}F+\widehat{\aleph}_{01}F+\widehat{q}^*_{01}=0, \quad (23) \tag{23}$$

$$\widehat{\mathcal{L}}_{02}\beta+\widehat{\mathfrak{R}}_{02}\beta+\widehat{\aleph}_{02}\beta+\widehat{q}^*_{02}=0, \quad (24) \tag{24}$$

In this stage, we define the Lagrange multipliers (j^* order of the model) for the velocity and temperature model equations.

$$\overset{\vee}{\lambda}_F=\frac{(-1)^{j^*}(\eta-s)^{j^*-1}}{(j^*-1)!}, \tag{25}$$

$$\overset{\vee}{\lambda}_\beta=\frac{(-1)^{j^*}(\eta-s)^{j^*-1}}{(j^*-1)!}, \tag{26}$$

Now, initial solutions for the model are described in the following way:

$$\overset{\vee}{F}_0=\sum_{i=0}^{r}\frac{\eta^iF(0)}{i!}\ \text{and}\ \overset{\vee}{\beta}_0=\sum_{i=0}^{r}\frac{\eta^i\beta(0)}{i!},$$

Finally, the analytical solution of the model computed according to the subsequent recursive formula and the accuracy of the solutions is subject to the number of iteration performed.

$$F_{l+1}=\overset{\vee}{F}_0+\int_0^\eta\overset{\vee}{\lambda}_F\left(-\overbrace{R_{01}}F(s)-\overbrace{\aleph_{01}}F(s)-\overbrace{q^*_{01}}(s)\right)ds,\ l\ge0,$$

$$\beta_{l+1}=\overset{\vee}{\beta}_0+\int_0^\eta\overset{\vee}{\lambda}_\beta\left(-\overbrace{R_{02}}\beta(s)-\overbrace{\aleph_{02}}\beta(s)-\overbrace{q^*_{02}}(s)\right)ds,\ l\ge0,$$

Results and discussion

The velocity and temperature distributions

This section describes the impact of hybrid nanofluid flow parameters, such as expanding/contracting parameter, magnetic parameter, permeable parameter, nanoparticle concentration, Reynolds number, Darcy number, and Forchheimer parameters on the velocity$F'(\eta)$. A comparative analysis of solution profiles for the nanofluid and hybrid nanofluid is presented in Figs. 4–6. In the figures, solid lines exemplify the solution for expanding channel, and the dotted lines embody the solution for contracting channel. Figure 4a and b shows a comparative movement of simple and hybrid nanoliquids for α and exhibits the evolution of fluid in the channel under increasing parametric values ofα. The contraction and expansion circumstances of the domain are recognized. The liquid particles possess optimum velocity about$\eta=0$. Physically, the wall expansion affords high working portion, and thus, the particles stroke is boosted. The fluid molecules are almost fluctuate near values of $\eta=-0.5$ and 0.5 for both nanoliquids. Physically, the contrary pressure resists the liquids movement in the surroundings of the walls. Therefore, the velocity increases slowly for hybrid nanoliquid due to frictional appearances and also looks declines in velocity near the walls according of boundary conditions. The 3D views are displayed in Fig. 4c and d. Figure 4e, f drawings the performance of the fluids on $F'(\eta)$ using a Hartmann number and displays that near $\eta \sim 0.5$, the fluid moves slowly due to reduced Ha but alters the influence before and after for both nanoliquids.

Figure 5a and b reveals the impacts of permutation factor 'S' on c for dual fluids. The appearance of permeability number 'S' is due to porous plates. The permeable state on walls of surface results in a substantial diminution in fluid movement. Therefore, for the growing values of S, the fluid moves gradually with controlled motion. Physically, for maximum number of porous region, the particles of fluid drag near the free space and hence reduce the movement in the region. Additionally, the motion of fluid can be handled by contracting the channel and compacting the permeable impacts, and Fig. 5c and d shows 3D trends. Figure 5e and f discourses the velocity profiles $F'(\eta)$ of (Ag-Go) nanofluids in absorptive channels for multiple levels of volume fraction ϕ_1. Graphically, it describes that the fluid's velocity escalations same as the volume fraction. Hence, the augmentation in velocity upon leading to the nanoparticles is due to nanoparticles' strange capacity to interchange rapidly inside the

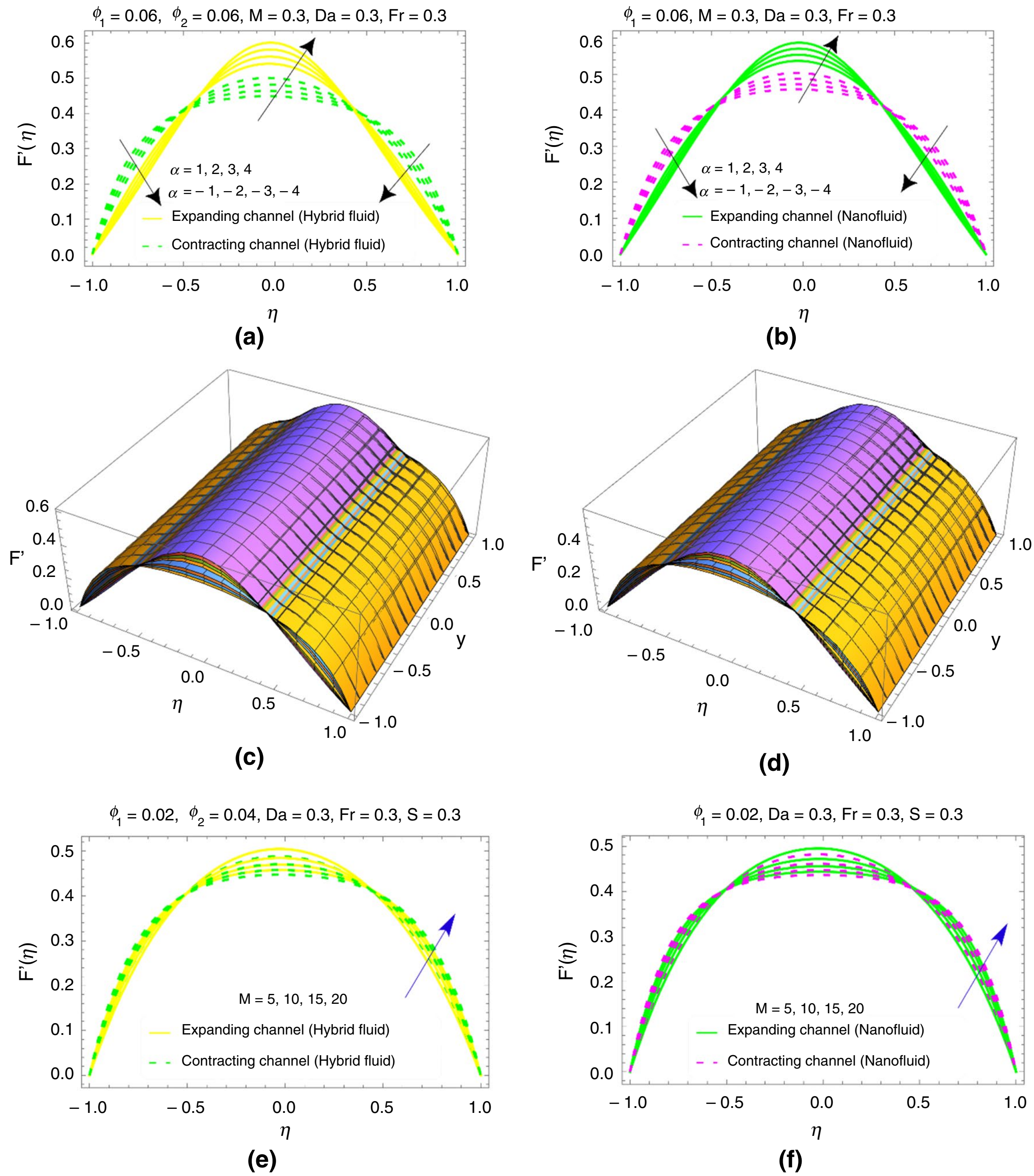

Fig. 4 The profile F′(η) against ‘α’ **a** hybrid and **b** nano, **c**, **d** 3D view of (**a**, **b**), and ‘M’ against **e** hybrid and **f** nano

fluid. It is well-known that Reynolds number is significant dimensionless number which effects the movement of liquid.

Figure 6a, b portrays the performance of $F'(\eta)$ for extending values of R_{e1} and displays that the fluid motion falls as the R_{e1} rises. But for HNF, these distinctions are very slow than the simple fluid. Physically, the simple fluid has stronger inertial forces than hybrid nanofluid that is worthy for rise in the movement. Figure 6c, d signifies the variations in the velocity $F'(\eta)$ as a function of D_a (Darcy number) and shows that near the lower plate, velocity abrupt strong increases with growth in constraint D_a but alteration point occurs near η ~ 0.5 and shows contrary behavior after this alteration point. It is recognized that Darcy number D_a exemplifies the relative influence of the absorptivity of the

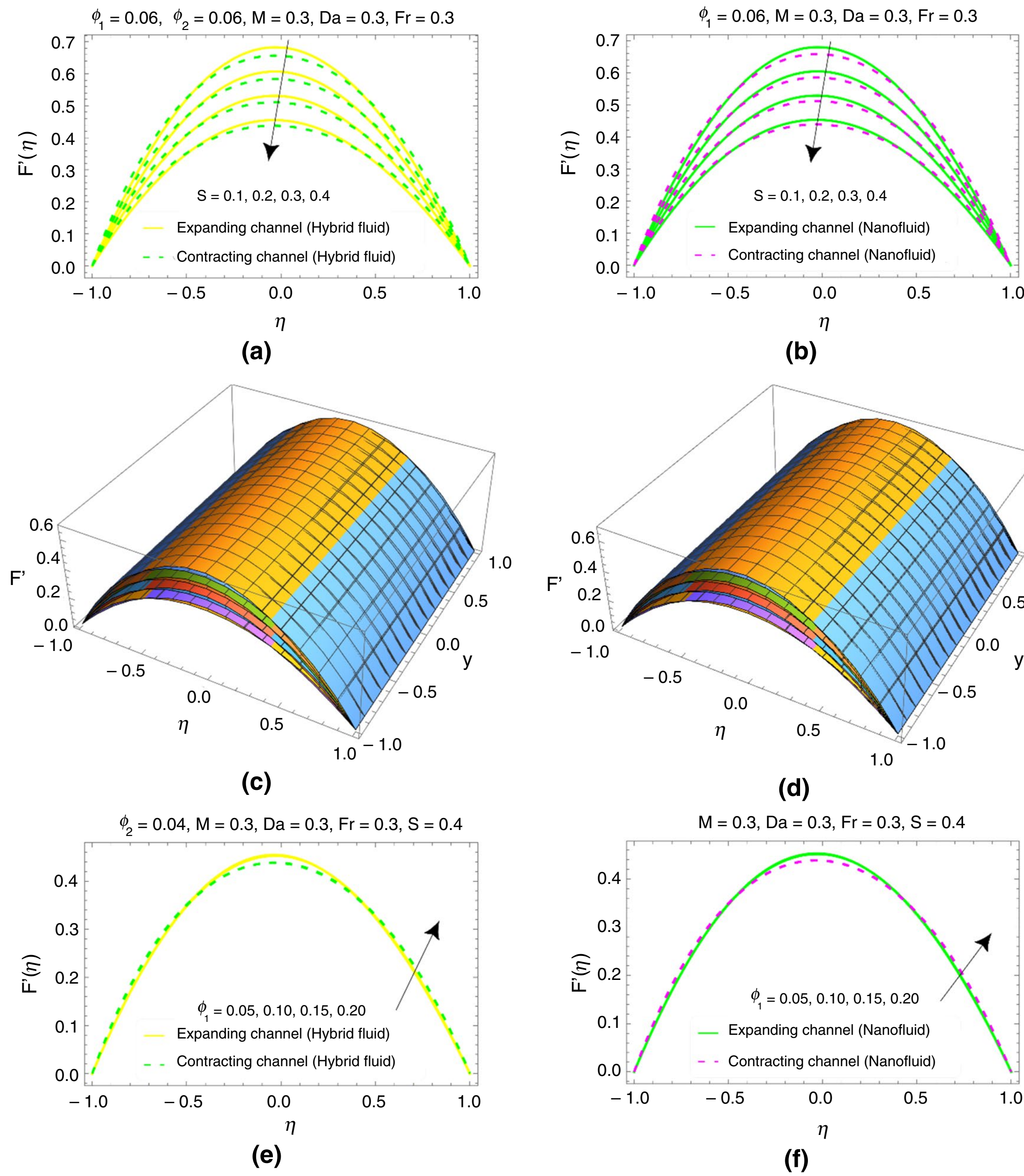

Fig. 5 The profile $F^{'}(\eta)$ against 'S' **a** hybrid and **b** nano, **c**, **d** 3D view of (**a**, **b**), and 'ϕ_1' against **e** hybrid and **f** nano

source versus the cross-sectional area of medium. While, absorptivity estimates the surface capability to flow over its membrane. The impact of Forchheimer parameter on dimensionless velocity is displays in Fig. 6e, f. It is experiential from graph that velocity growth as the Forchheimer number escalates. The purpose for this behavior is that inertia of permeable medium contributes an additional detention to the fluid flow mechanism, which causes the fluid to move and hence velocity increases.

Figures 7–9 exhibit the changes in temperature with alteration of involved parameters. The influence of expansion/contraction parameter α on $F\prime$ is displayed in Fig. 7a, b. It is disclosed from graph that temperature profile $\beta(\eta)$ decreases with increasing values of parameter. Figure 7c, d reveals the upshots of temperature when the 'heat generation/absorption

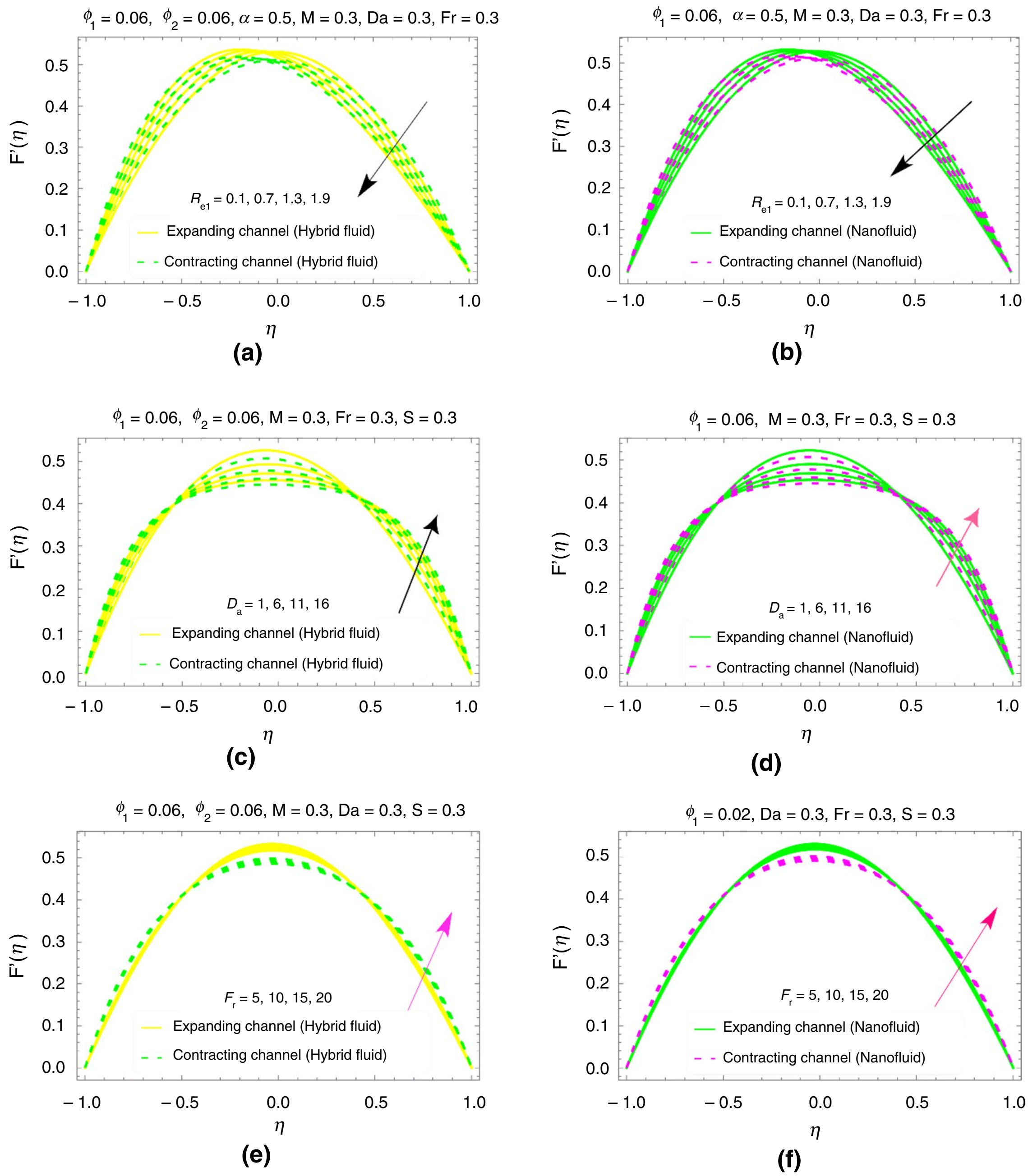

Fig. 6 The profile $F'(\eta)$ against 'R_{e1}' **a** bi-hybrid and **b** nano, 'D_a' **c** bi-hybrid and **d** nano, and 'F_r' against **e** bi-hybrid and **f** nano

parameter' Q increases. The higher assessments of a mentioned parameter results in temperature to raise. The enlargement in parameter Q suggests the generation of heat in the modeled system and variations correspond to more quantities of heat being produced. Hence, the temperature $\beta(\eta)$ upsurges with developed assessments of the heat generation parameter. Figure 7e, f establishes the variation tendency of non-dimensional temperature $\beta(\eta)$ due to fluctuating in permeable parameter S for porous surface, and the decrease in $\beta(\eta)$ is observed when parameter S is increased. Graphically, it is observed that the heating performance of bi-hybrid nanoliquid is more visible than the simple nanofluid.

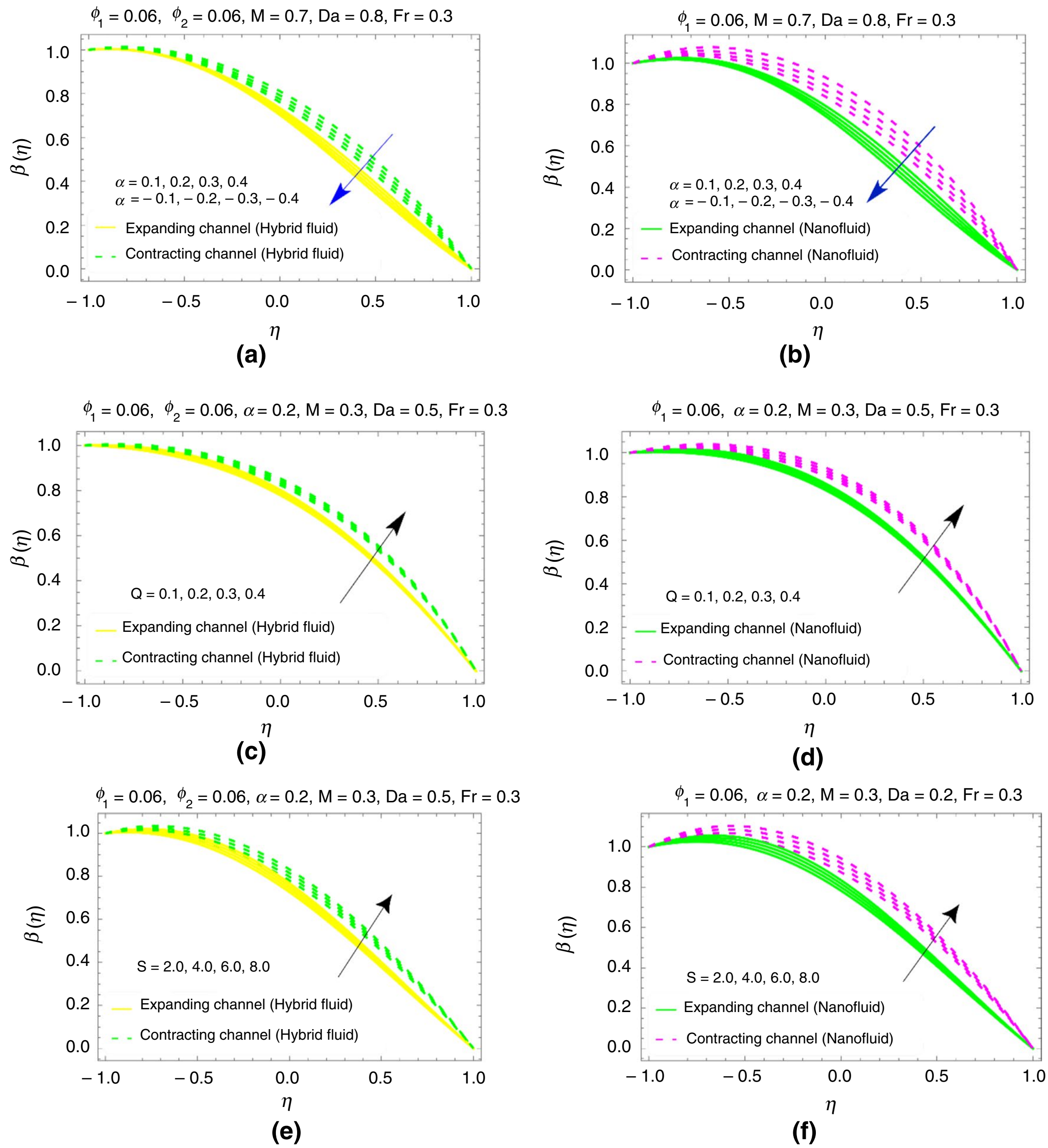

Fig. 7 The profile β(η) against 'α' **a** bi-hybrid and **b** nano, 'Q' **c** bi-hybrid and **d** nano, and 's' against **e** bi-hybrid and **f** nano

Figure 8a, b demonstrates the deviate behavior in temperature $\beta(\eta)$ for varying M. It is apparent from graph that the improvement in the parameter M declines the temperature in dual cases. The Lorentz force prevents the mobility of fluid which gives a diminution in the thermal diffusion, and Fig. 8c, d shows 3D view. Nanoparticle fraction effect is detected from Fig. 8e, f which depicts that temperature distribution declines due to increasing values of parameter. As ϕ1 varies, the intermolecular distance is reduced among simple fluid and hybrid nanoparticles which causes augmented the resistance of flow viscosity of fluid which causes a decrement in temperature as specified in Fig. 8e, f. The increasing R_{e1} on temperature field is exposed in Fig. 9a, b and is depicts that temperature $\beta(\eta)$ growths as Reynolds number parameter varies. Figure 9c,

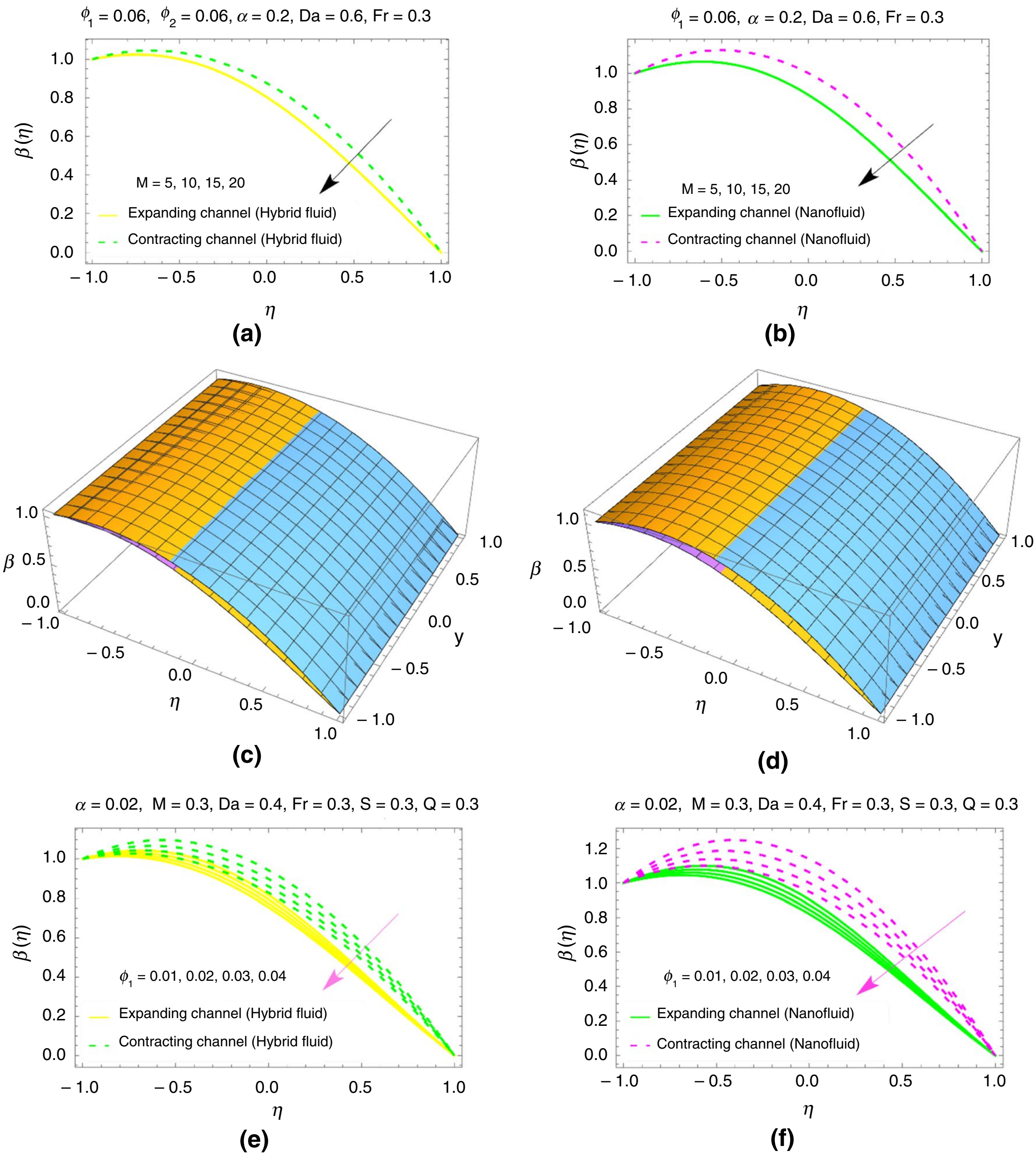

Fig. 8 The profile $\beta(\eta)$ against 'M' **a** bi-hybrid and **b** nano, (**c**, **d**) 3D view of (**a**, **b**), and 'ϕ_1' against **e** bi-hybrid and **f** nano

d is plotted to locate the impact of Darcy number parameter D_a on temperature profile. It is recognized from figure that increasing the Darcy number parameter is decreased for simple and hybrid base fluid, respectively.

Tabulated results

The computational results for the local thermal gradient and shear drag for (Ag-Go)/water hybrid nanofluid are described under this subsection and the calculated for both walls. Table 2 indicates that with addition of GO nanoparticles in blood, the shear drag rises but it is optimized with contraction of plates. Furthermore, the absolute estimation of shear drag upsurges at top of wall. The estimation revealed that the R_{e1} is main factor to attain extreme shear drags according to other constraints.

Table 3 determines the performance of Nu for hybrid nanoliquid under model quantities. The profound analysis

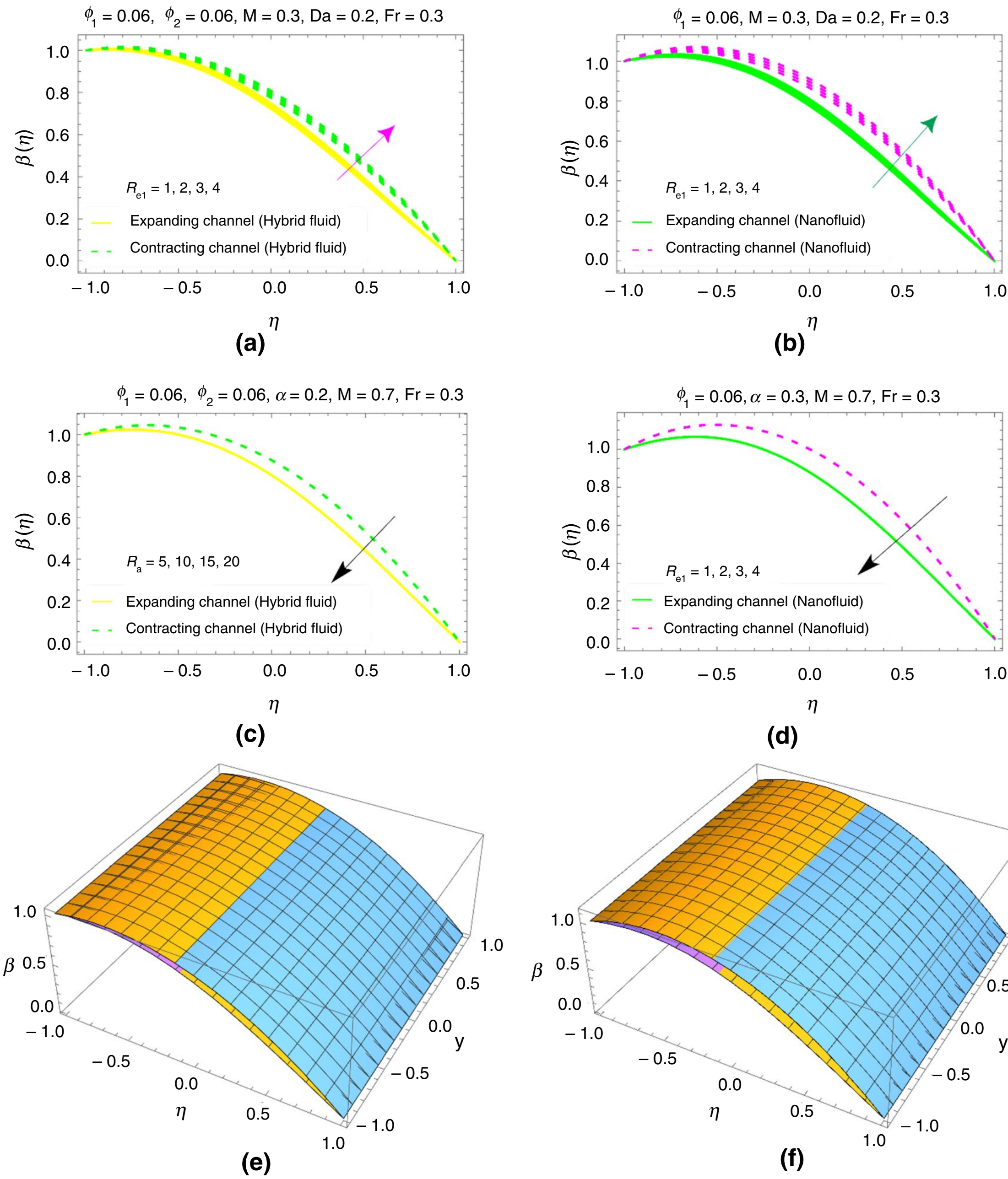

Fig. 9 The profile β(η) against 'R_{e1}' **a** Hybrid **b** nano, 'D_a' against **e** Hybrid **f** Nano (**c**, **d**) 3D view of (**a**, **b**)

designates that inflation of the particles 1–40% is capable to achieved optimum Nu but it dominates at top end. Further, Fig. 10 highlighting the streamlines pattern and isotherms for the present problem.

Model validation

The replication of the problem results is of paramount interest in the scientific literature. Therefore, this subsection fixed to provide the current model validity by comparing it results with the reported data. Thus, the present modified model results under no Lorentz forces, zero nanoparticles concentration, and in non-Darcy medium are furnished and compared the results of Majdalani et al. [56]. The comparative plotted results in Fig. 11a–d ensure that the model results are accurately aligned with the data of Majdalani et al. [56]. The results exhibited for both expanding and contracting cases and found a very good agreement to those of Majdalani et al. [56]. This proves the reliability of the model and its further results in the subsequent section.

Table 2 Computations of skin friction for bottom and top end of the channel verses various values of physical constraints

Parameters values								Shear drag values			
ϕ_1	ϕ_2	a	M	D_a	F_r	S	R_{e1}	$F''(-1)$		$\lvert F''(1)\rvert$	
	0.03	0.3	3.0	0.5	0.5	0.3	0.2	Expansion	Contraction	Expansion	Contraction
0.01								0.9118	0.9875	0.8488	0.9193
0.02								0.9134	0.9889	0.8507	0.9210
0.03								0.9150	0.9903	0.8526	0.9227
0.04								0.916	0.9917	0.8547	0.9245
0.01	0.01							0.9300	0.9998	0.8726	0.9381
	0.02							0.9203	0.9932	0.8601	0.9281
	0.03							0.9118	0.9875	0.8488	0.9193
	0.04							0.9043	0.9827	0.8388	0.9114
	0.03	0.1						0.9362	0.9614	0.8715	0.8950
		0.2						0.9239	0.9744	0.8601	0.9070
		0.3						0.9118	0.9875	0.8488	0.9193
		0.4						0.8999	1.0009	0.8378	0.9318
		0.3	1.0					0.8668	0.8917	0.7973	0.8203
			2.0					0.8898	0.9400	0.8239	0.8703
			3.0					0.9118	0.9875	0.8488	0.9193
			4.0					0.9327	1.0342	0.8724	0.9672
			3.0	0.2				0.8529	0.8778	0.7824	0.8052
				0.3				0.8454	0.8953	0.7763	0.8220
				0.4				0.8381	0.9129	0.7704	0.8391
				0.5				0.8310	0.9308	0.7646	0.8563
				0.5	0.1			0.8655	0.8905	0.7960	0.8189
					0.2			0.8537	0.9036	0.7852	0.8310
					0.3			0.8421	0.9169	0.7746	0.8434
					0.4			0.8306	0.9305	0.7643	0.8560
					0.5	0.1		1.1068	1.1385	1.0316	1.0612
						0.3		0.8546	0.9045	0.7862	0.8321
						0.5		0.6060	0.6601	0.5502	0.5992
						0.7		0.3610	0.4047	0.3234	0.3625
						0.3	0.2	0.8668	0.8917	0.7973	0.8203
							0.4	0.8897	0.9411	0.7553	0.7987
							0.6	0.9127	0.9920	0.7173	0.7790
							0.8	0.9354	1.0441	0.6831	0.7610

Table 3 Nu computations for bottom and top end of the channel verses various values of physical constraints

ϕ_1	Parameters values ϕ_2 0.03	α 0.1	M 0.3	D_a 0.5	F_r 0.5	S 0.3	Q 0.3	R_{e1} 0.2	Heat transfer gradient variations $\lvert\beta'(-1)\rvert$ Expansion	$\lvert\beta'(-1)\rvert$ Contraction	$\lvert\beta'(1)\rvert$ Expansion	$\lvert\beta'(1)\rvert$ Contraction
0.02									0.8281	1.1199	1.6767	2.1987
0.04									0.6419	0.8319	1.5196	1.9142
0.06									0.4876	0.6112	1.3910	1.6966
0.08									0.3582	0.4371	1.2841	1.5255
0.02	0.01								0.9402	1.3055	1.7721	2.3826
	0.03								0.8281	1.1199	1.6767	2.1987
	0.05								0.7281	0.9621	1.5921	2.0425
	0.07								0.6382	0.8262	1.5165	1.9083
	0.03	0.1							0.8281	1.1199	1.6767	2.1987
		0.2							0.7241	1.3255	1.4724	2.5351
		0.3							0.6398	1.5885	1.2969	2.9402
		0.4							0.5710	1.9295	1.1455	3.4345
		0.1	0.1						0.8281	1.1199	1.6769	2.1988
			0.2						0.8281	1.1199	1.6768	2.1988
			0.3						0.8281	1.1199	1.6767	2.1987
			0.4						0.8281	1.1199	1.6767	2.1986
			0.3	0.1					0.8281	1.1199	1.6771	2.1991
				0.4					0.8281	1.1199	1.6768	2.1988
				0.7					0.8282	1.1199	1.6766	2.1985
				1.0					0.8282	1.1199	1.6764	2.1982
				0.5	0.2				0.8281	1.1199	1.6768	2.1987
					0.4				0.8281	1.1199	1.6767	2.1987
					0.6				0.8281	1.1199	1.6767	2.1987
					0.8				0.8281	1.1199	1.6767	2.1987
					0.5	0.1			0.7117	0.9721	1.6162	2.1120
						0.2			0.7699	1.0460	1.6465	2.1554
						0.3			0.8281	1.1199	1.6767	2.1987
						0.4			0.8863	1.1936	1.7069	2.2419
						0.3	0.1		0.0774	0.1116	1.1626	1.4368
							0.2		0.4080	0.5404	1.3774	1.7452
							0.3		0.8281	1.1199	1.3774	2.1987
							0.4		1.3955	1.9755	2.1176	2.9221
							0.3	0.1	0.5863	0.7881	1.3371	1.7600
								0.2	0.8281	1.1199	1.6767	2.1987
								0.3	1.0714	1.4537	2.0178	2.6394
								0.4	1.3160	1.7894	2.3601	3.0819

Fig. 10 Contour Upshots/(Streamline and isothermal) in **a**–**j** due to variations in various physical constraints

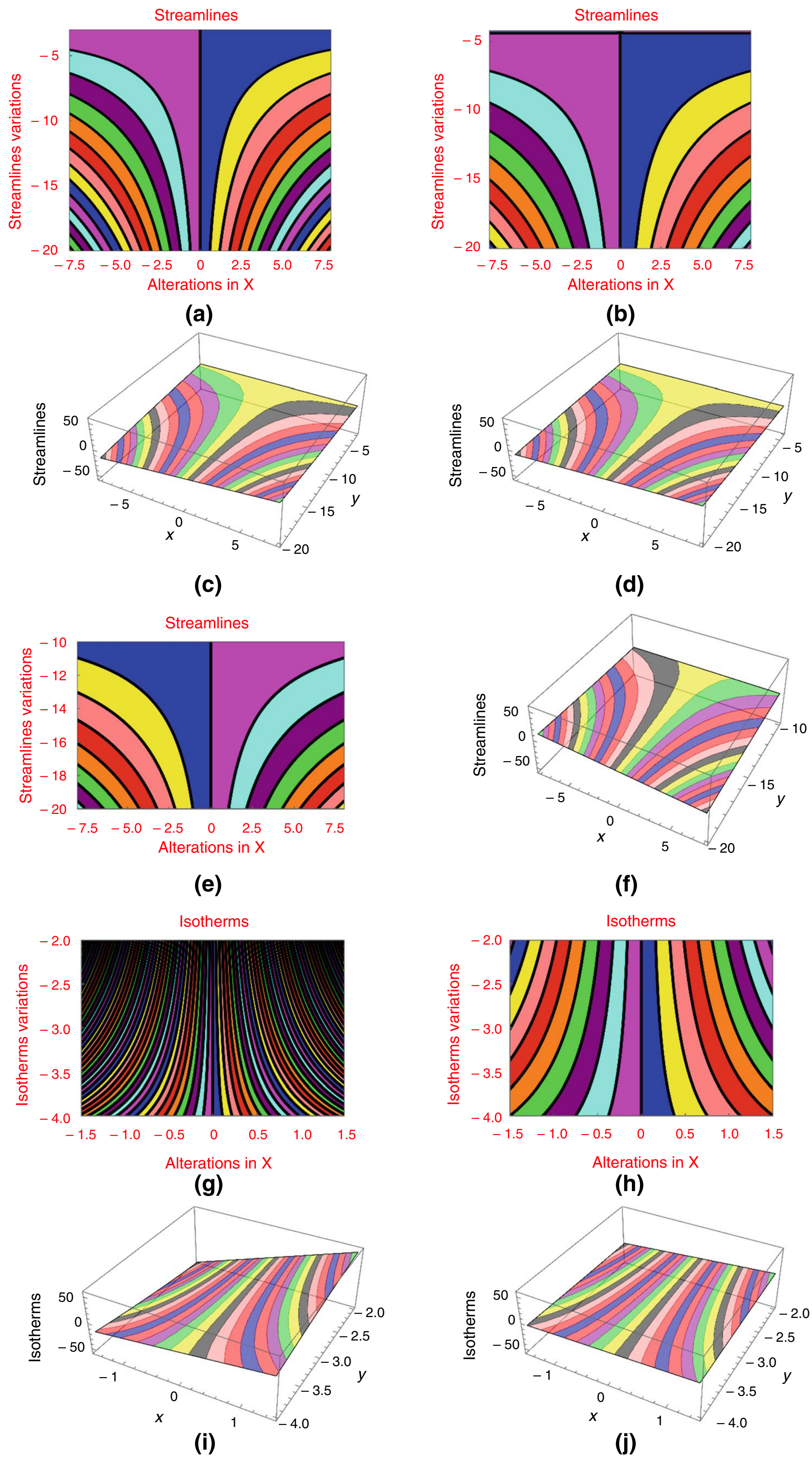

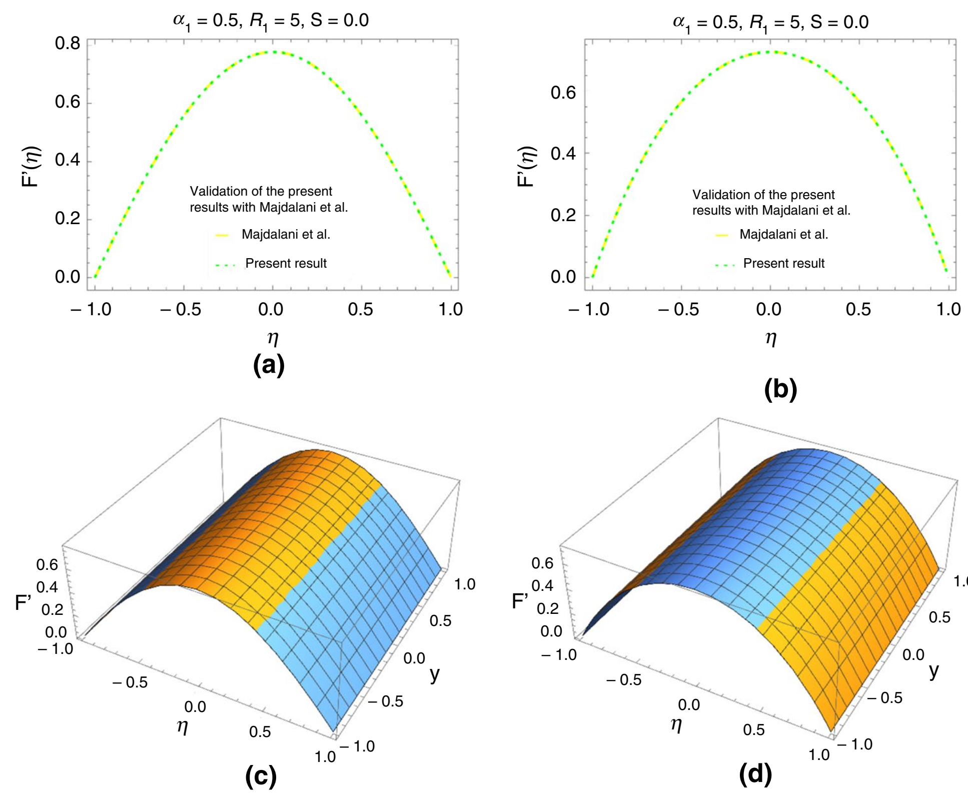

Fig. 11 The present model validation with the published scientific data

Conclusions

The study of hybrid nanofluid in a channel containing two plates is presented. The problem formulation has been done by keeping hybrid nanofluid effective characteristics and similarity transformative rules under consideration. The acquired model investigates via semi-analytical scheme (variational iteration method) and then influences of ingrained physical quantities on the problem dynamics which are simulated and discussed from the physical aspects. It is scrutinized that:

- The movement of hybrid and simple nanofluids under increasing expanding/contracting number $\alpha = 1.0, 2.0, 3.0, 4.0$ and $\alpha = -1.0, -2.0, -3.0, -4.0$ drops toward the walls, and it upsurges in the middle of the channel.
- The uniform injection of the fluid from the pores present at the walls highly reduced the fluid motion, and rapid declines are observed about $\eta = 0.0$ which represents the middle area of the channel.
- The increasing strength of magnetic field ($M = 5.0, 10.0, 15.0, 20.0$) and Darcy effects resists the movement of hybrid and conventional nanofluids. Thus, directed magnetic field on the permeable channel is a good source to control the working fluid motion.
- The fluid particles move very slowly under higher Forchheimer effects for both types of considered nanofluids.
- The heat generation number $Q = 0.1, 0.2, 0.3, 0.4$ positively enhanced the temperature of both sort of fluids and is examined rapid for contracting channel case.
- The higher magnetic field and strong expansion/contraction of the walls are the sources to diminish the hybrid and nanofluids temperature.

In the future, the study could be extended for various engineered nanofluids comprising aluminum alloys, carbon nanotubes, and other metallic and nonmetallic nanoparticles in the presence of potential physical constituents.

Acknowledgements The authors extend their appreciation to the Deanship of Scientific Research at King Khalid University for funding this work through large group Research Project under grant number RGP2/16/44.

Data availability The data that support the findings of this study are available within the article.

Declarations

Conflict of interest There is no financial/competing interest regarding the publication of this work.

References

1. Ali B, Jubair S, Al-Essa LA, Mahmood Z, Al-Bossly A, Alduais FS. Boundary layer and heat transfer analysis of mixed convective nanofluid flow capturing the aspects of nanoparticles over a needle. Mater Today Commun. 2023;35. https://doi.org/10.1016/j.mtcomm.2023.106253.
2. Bilal A, Duraihem FZ, Sidra J, Alqahtani H, Yagoob B. Analysis of Interparticle spacing and nanoparticle radius on the radiative alumina based nanofluid flow subject to irregular heat source/sink over a spinning disk. Material Today Commun. 2023. https://doi.org/10.1016/j.mtcomm.2023.106729.
3. Ali B, Mishra NK, Rafique K, Jubair S, Zafar M, Eldin SM. Mixed convective flow of hybrid nanofluid over a heated stretching disk with zero-mass flux using the modified Buongiorno model. Alexandria Eng J. 2023;83–96.
4. Mustafa M, Mushtaq A, Hayat T, Ahmad B. Nonlinear radiation heat transfer effects in the natural convective boundary layer flow of nanofluid past a vertical plate: a numerical study. PLoS ONE. 2014;9. https://doi.org/10.1371/journal.pone.0103946.
5. Hosseinzadeh K, Amiri AJ, Ardahaie SS, Ganji DD. Effect of variable lorentz forces on nanofluid flow in movable parallel plates utilizing analytical method. Case Stud Thermal Eng. 2017;10. 595–10.
6. Adnan. Heat transfer inspection in [(ZnO-MWCNTs)/water-EG(50:50)]hnf with thermal radiation ray and convective condition over a Riga surface. Waves Random Complex Media. 2022. https://doi.org/10.1080/17455030.2022.2119300.
7. Alharbi KAM, Adnan, A. M. Galal. Novel magneto-radiative thermal featuring in SWCNT–MWCNT/$C_2H_6O_2$–H_2O under hydrogen bonding. Int J Mod Phys B. 2023. https://doi.org/10.1142/S0217979224500176.
8. Rafique k, Mahmood Z, Alqahtani H, Eldin SM. Various nanoparticle shapes and quadratic velocity impacts on entropy generation and MHD flow over a stretching sheet with joule heating. Alexandria Eng J. 2023. vol. 71.147–59.
9. Bilal A, Jubair S, Fathima D, Akhter A, Khadija K, Zafar M. MHD flow of nanofluid over moving slender needle with nanoparticles aggregation and viscous dissipation effects. Sci Prog. 2023. https://doi.org/10.1177/00368504231176151.
10. Mishra NK, Adnan, Sarfraz G, Bani-Fwaz MZ, Eldin SM. Dynamics of Corcione nanoliquid on a convectively radiated surface using Al_2O_3 nanoparticles. J Thermal Anal Calorimetry. 2023. https://doi.org/10.1007/s10973-023-12448-y.
11. Bhatti MM, Sait SM, Ellahi R, Sheremet MA, Oztop H. Thermal analysis and entropy generation of magnetic Eyring-Powell nanofluid with viscous dissipation in a wavy asymmetric channel. Int J Numer Methods Heat Fluid Flow. 2023;33:1609–36.
12. Zhang L, Tariq N, Bhatti MM. Study of nonlinear quadratic convection on magnetized viscous fluid flow over a non-Darcian circular elastic surface via spectral approach. J Taibah Univ Sci. 2023. https://doi.org/10.1080/16583655.2023.2183702.
13. Kumar NM, Adnan, Sohail MU, Hassan AM. Thermal analysis of radiated (aluminum oxide)/water through a magnet based geometry subject to Cattaneo-Christov and Corcione's Models. Case Stud Thermal Eng. 2023;49. https://doi.org/10.1016/j.csite.2023.103390.
14. Nidhish NM, Adnan, Rahman KU, Fwaz MZB. Investigation of blood flow characteristics saturated by graphene/CuO hybrid nanoparticles under quadratic radiation using VIM: study for expanding/contracting channel. Sci Rep. 2023;13. https://doi.org/10.1038/s41598-023-35695-3.
15. Madhukesh JK, Ramesh GK, Roopa GS, Prasannakumara BC, Shah NA, Yook SJ. 3D flow of hybrid nanomaterial through a circular cylinder: saddle and nodal point aspects. Mathematics. 2022;10. https://doi.org/10.3390/math10071185.
16. Gowda RJP, Rauf A, Kumar RN, Prasannakumara BC, Shehzad SA. Slip flow of Casson–Maxwell nanofluid confined through stretchable disks. Ind J Phys. 2022; 96:2041–49.
17. Kumar RN, Suresha S, Gowda RJP, Megalamani SB, Prasannakumara BC. Exploring the impact of magnetic dipole on the radiative nanofluid flow over a stretching sheet by means of KKL model. Pramana. 2021;95. https://doi.org/10.1007/s12043-021-02212-y.
18. Murtaza S, Kumam P, Ahmad KZ, Ramzan M, Ali I, Saeed A. Computational simulation of unsteady squeezing hybrid nanofluid flow through a horizontal channel comprised of metallic nanoparticles. J Nanofluids. 2023;12:1327–34.
19. Khan N, Ali F, Ahmad Z, Murtaza S, Ganie AH, Khan I, Eldin SM. A time fractional model of a Maxwell nanofluid through a channel flow with applications in grease. Sci Rep. 2023;13. https://doi.org/10.1038/s41598-023-31567-y.
20. Ali F, Ahmad Z, Arif M, Khan I, Nisar K. a time fractional model of generalized couette flow of couple stress nanofluid with heat and mass transfer: applications in engine oil. IEEE Access. 2020. https://doi.org/10.1109/ACCESS.2020.3013701.
21. Bano A, Dawood A, Rida, Saira F, Malik A, Alkholief M, Ahmad HMA, Ahmad Z, Bazighifan O. Enhancing catalytic activity of gold nanoparticles in a standard redox reaction by investigating the impact of AuNPs size, temperature and reductant concentrations. Sci Rep. 2023;13. https://doi.org/10.1038/s41598-023-38234-2.
22. Murtaza S, Zubair A, Ali IE, Akhtar Z, Tchier F, Ahmad H, Yao SW. Analysis and numerical simulation of fractal-fractional order non-linear couple stress nanofluid with cadmium telluride nanoparticles. J King Saud Univ Sci. 2023;35. https://doi.org/10.1016/j.jksus.2023.102618.
23. Hasin F, Ahmad Z, Ali F, Khan N, Khan I, Eldin SM. Impact of nanoparticles on vegetable oil as a cutting fluid with fractional ramped analysis. Sci Rep. 2023. https://doi.org/10.1038/s41598-023-34344-z.
24. Sharma A, Dubewar AV. MHD flow between two parallel plates under the influence of inclined magnetic field by finite difference method. Int J Innov Technol Explor Eng. 2019;8. https://doi.org/10.35940/ijitee.L3643.1081219.
25. Abbas W, Magdy MM. Heat and mass transfer analysis of nanofluid flow based on Cu, Al2O3, and TiO2 over a moving rotating plate and impact of various nanoparticle shapes. Math Probl Eng. 2020. https://doi.org/10.1155/2020/9606382.
26. Ali K, Ahmad A, Ahmad S, Nisar KS, Ahmad S. Peristaltic pumping of MHD flow through a porous channel: biomedical engineering application. Waves Random Complex Media. 2023. https://doi.org/10.1080/17455030.2023.2168085.
27. Zhang X, Yang D, Kashif A, Faridi AA, Ahmad S, Jamshed W, Raezah AA, El Din SM. Successive over relaxation (SOR) methodology for convective triply diffusive magnetic flowing via a porous horizontal plate with diverse irreversibilities. Ain Shams Eng J. 2023;14. https://doi.org/10.1016/j.asej.2023.102137.
28. Zainal NA, Nazar R, Naganthran K, Pop I. Stability analysis of MHD hybrid nanofluid flow over a stretching/shrinking sheet with quadratic velocity. Alexandria Eng J. 2020;60. 915–26.
29. Akbar S, Hussain A. The Influences of squeezed inviscid flow between parallel plates. Math Probl Eng. 2021. https://doi.org/10.1155/2021/6647708.
30. Mishra NK, Khalid AMA, Rahman KU, Adnan A, Eldin SM, Fwaz MZB. Investigation of improved heat transport featuring in dissipative ternary nanofluid over a stretched wavy cylinder under thermal slip. Case Stud Thermal Eng. 2023;48. https://doi.org/10.1016/j.csite.2023.103130.
31. Ahmad S, Ashraf M, Ali K. Simulation of thermal radiation in a micropolar fluid flow through a porous medium between channel walls. J Thermal Anal Calorimetry. 2021;941–53.

32. AL-Zahrani AA, Adnan A, Mahmood I, Khaleeq RU, Mutasem ZBF, Tag-Eldin E. Analytical study of (Ag–graphene)/blood hybrid nanofluid influenced by (platelets-cylindrical)nanoparticles and joule heating via VIM. ACS Omega. 2023;8:19926–38.
33. Kashif A, Ahmad S, Nisar KS, Faridi AA, Ashraf M. Simulation analysis of MHD hybrid CuAl2O3/H2O nanofluid flow with heat generation through a porous media. Int J Energy Res. 2021. https://doi.org/10.1002/er.7016.
34. Noor AAM, Shafie S, Admon MA. Heat and mass transfer on MHD squeezing flow of Jeffrey nanofluid in horizontal channel through permeable medium. PLOS One. 2021;16. https://doi.org/10.1371/journal.pone.0250402.
35. Hussain A, Alshbool MH, Abdussattar A, Rehman A, Ahmad H, Nofal T, Khan MR. A computational model for hybrid nanofluid flow on a rotating surface in the existence of convective condition. Case Stud Thermal Eng. 2021;26. https://doi.org/10.1016/j.csite.2021.101089.
36. Waqas H, Farooq U, Naseem R, Hussain S, Alghamdi M. Impact of MHD radiative flow of hybrid nanofluid over a rotating disk. Case Stud Thermal Eng. 2021;26. https://doi.org/10.1016/j.csite.2021.101015.
37. Ahammad NA, Badruddin IA, Kamangar S, Khaleed HMT, Saleel CS, Mahila TMI. Heat transfer and entropy in a vertical porous plate subjected to suction velocity and MHD. Entropy. 2021. https://doi.org/10.3390/e23081069.
38. Adnan A, Abbas W, Sayed ME, Mutasem ZBF. Numerical investigation of non-transient comparative heat transport mechanism in ternary nanofluid under various physical constraints. AIMS Math. 2023;8:15932–49.
39. Abdullah MR, Khawatreh SA. Unsteady MHD flow and heat transfer through porous medium between parallel plates with periodic magnetic field and constant pressure gradient. Int J Eng Res Technol. 2021;14:782–87
40. Rashad AM, Nafe MA, Eisa DA. Heat Generation and Thermal Radiation Impacts on Flow of Magnetic Eyring–Powell Hybrid Nanofluid in a Porous Medium. Arab J Sci Eng. 2022. vol. 48. 939–52.
41. Abdulkhaliq KAM, Adnan A, Akgul A. Investigation of Williamson nanofluid in a convectively heated peristaltic channel and magnetic field via method of moments. AIP Adv. 2023;13. https://doi.org/10.1063/5.0141498.
42. Yaseen M, Rawat SK, Shafiq A, Kumar M, Nonlaopon K. Analysis of heat transfer of mono and hybrid nanofluid flow between two parallel plates in a darcy porous medium with thermal radiation and heat generation/absorption. Symmetry. 2022. https://doi.org/10.3390/sym14091943.
43. Alhowaity A, Bilal M, Hamam H, Alqarni MM, Mukdasai K, Aatif A. Non-Fourier energy transmission in power-law hybrid nanofluid flow over a moving sheet. Sci Rep. 2022. https://doi.org/10.1038/s41598-022-14720-x.
44. Muhammad B, Ali A, Hejazi HA, Mahmuod SR. Numerical study of an electrically conducting hybrid nanofluid over a linearly extended sheet. J Appl Math Mech. 2022. https://doi.org/10.1002/zamm.202200227.
45. Alqahtani AM, Bilal M, Usman M, Alsenani TR, Samy RM, Ali A. Heat and mass transfer through MHD Darcy Forchheimer Casson hybrid nanofluid flow across an exponential stretching sheet. J Appl Math Mech. 2023. https://doi.org/10.1002/zamm.202200213.
46. Haq I, Bilal M, Ahammad NA, Ghoneim ME, Weera W. Mixed convection nanofluid flow with heat source and chemical reaction over an inclined irregular surface. ACS Omega. 2022;30477–85.
47. Abbas N, Shatanawi W, Shatnawi TAM. Transportation of nanomaterial Maxwell fuid fow with thermal slip under the efect of Soret-Dufour and second-order slips: nonlinear stretching. Sci Rep. 2023. https://doi.org/10.1038/s41598-022-25600-9.
48. Zeighami LAF, Federico V. Efective forchheimer coefcient for layered porous media. Transp Porous Media. 2022. https://doi.org/10.1007/s11242-022-01815-2.
49. Elbashbeshy EMA, Asker HG. Fluid flow over a vertical stretching surface within a porous medium filled by a nanofluid containing gyrotactic microorganisms. Eur Phys J Plus. 2022. https://doi.org/10.1140/epjp/s13360-022-02682-y.
50. Adnan A, Alharbi KAM, Bani-Fwaz MZ, Eldin SM, Yassen MF. Numerical heat performance of TiO_2/Glycerin under nanoparticles aggregation and nonlinear radiative heat flux in dilating/squeezing channel. Case Stud Therm Eng. 2023;41. https://doi.org/10.1016/j.csite.2022.102568.
51. Nadeem A, Adnan A, Sayed ME. Heat transport mechanism in glycerin-titania nanofluid over a permeable slanted surface by considering nanoparticles aggregation and Cattaneo Christov thermal flux. Sci Prog. 2023. https://doi.org/10.1177/00368504231180032.
52. Kumar RN, Gowda RJP, Alam MM, Ahmad I, Mahrous YM, Gorji MR, Prasannakumara BC. Inspection of convective heat transfer and KKL correlation for simulation of nanofluid flow over a curved stretching sheet. Int Commun Heat Mass Transf. 2021. https://doi.org/10.1016/j.icheatmasstransfer.2021.105445.
53. Kumar RSV, Alhadhrami A, Gowda RJP, Kumar RN, Prasannakumara BC. Exploration of arrhenius activation energy on hybrid nanofluid flow over a curved stretchable surface. ZAMM. 2021. https://doi.org/10.1002/zamm.202100035.
54. Rekha MB, Sarris IE, Madhukesh JK, Prasannakumara BC. Activation energy impact on flow of aa7072-aa7075/water-based hybrid nanofluid through a cone, wedge and plate. Micromachines. 2022;13. https://doi.org/10.3390/mi13020302.
55. Saeed A, Tassaddiq A, Khan A, Jawad M, Deebani W, Shah Z, Islam S. Darcy–Forchheimer MHD hybrid nanofluid flow and heat transfer analysis over a porous stretching cylinder. Coatings. 2020;10. https://doi.org/10.3390/coatings10040391.
56. Majdalani J, Zhou C, Dawson CA. Two-dimensional viscous flow between slowly expanding or contracting walls with weak permeability. J Biomech. 2002;35:1399–03.
57. Shi QH, Hamid A, Khan MI, Kumar RN, Gowda RJP, Prasannakumara BC, Shah NA, Khan SU, Chung JD. Numerical study of bio-convection flow of magneto-cross nanofluid containing gyrotactic microorganisms with activation energy. Sci Rep. 2021. https://doi.org/10.1038/s41598-021-95587-2.